THE JOURNAL OF PHYSICAL CHEMISTRY C

Article

pubs.acs.org/JPCC

Distribution of 1-Butyl-3-methylimidazolium Bistrifluoromethylsulfonimide in Mesoporous Silica As a Function of Pore Filling

Kee Sung Han, Xiqing Wang, Sheng Dai, and Edward W. Hagaman*

Chemical Sciences Division, Oak Ridge National Laboratory, Oak Ridge, Tennessee 37831, United States

Supporting Information

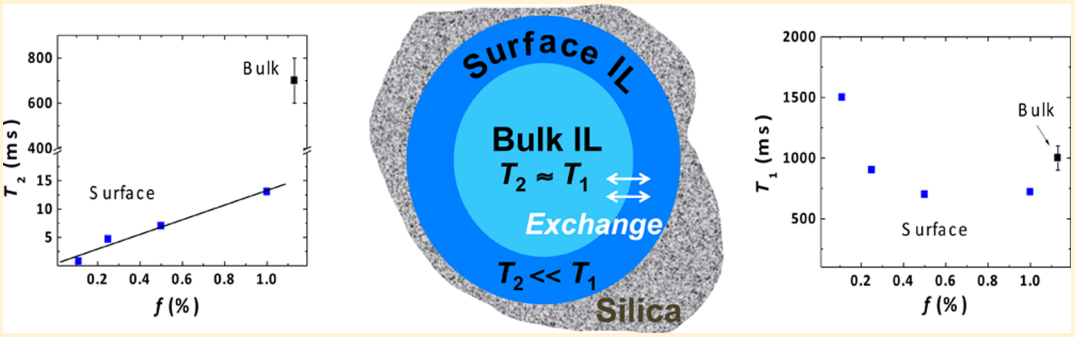

ABSTRACT: Rotational dynamics of the ionic liquid (IL) 1-butyl-3-methylimidazolium bistrifluoromethylsulfonimide, [C_4mim][Tf_2N], **1**, as a neat liquid, and confined in mesoporous silica were investigated by ^{1}H spin−spin (T_2) and spin−lattice (T_1) relaxation measurements and ^{13}C NMR spectroscopy. Translational dynamics (self-diffusion) were monitored via the diffusion coefficient, D, obtained with ^{1}H pulsed field gradient NMR measurements. These data were used to determine the distribution of **1** in the pores of KIT-6, a mesoporous silica with a bicontinuous gyroid pore structure, as a function of filling fraction. Relaxation studies performed as a function of filling factor and temperature reveal a dynamic heterogeneity in both translational and rotational motions for **1** at filling factors, f = 0.2−1.0 (f = 1 corresponds to fully filled pores). Spin−lattice and spin−spin relaxation times reveal that the motion of **1** in silica mesopores conforms to that expected for a two-dimensional relaxation model. The relaxation dynamics are interpreted using a two-state, fast exchange model for all motions; a slow rotation (and translation) of molecules in contact with the surface and a faster motion approximated by the values for bulk relaxation and diffusion. Compound **1** retains liquid-like behavior at all filling factors and temperatures that extend to ca. 50 degrees below the bulk melting point. Translational motion in these systems, interpreted with MD-simulated diffusivity limits, confirms the high propensity of **1** to form a monolayer film on the silica surface at low filling factors. The attractive interaction of **1** with the surface is greater than that for self-association of **1**. The trends in diffusion data at short and long diffusion time suggest that the population of surface-bound **1** is in intimate contact with **1** in the pores. This condition is most easily met at higher filling fractions with successive additions of **1** increasing the layer thickness built up on the surface layer.

INTRODUCTION

The structure and dynamics of room temperature ionic liquids (RTILs) at the fluid/solid interface have gained attention due to their potential applications as components of energy storage devices such as batteries, capacitors, fuel cells , and solar cells, and as electrochemical sensors, biosensors, and drug release systems.[1,2] In confinement, the well-known properties of bulk ILs such as high ionic conductivity, thermal and chemical stability, nonflammability, and nonvolatility[3] are influenced by the host material interfaces. Molecular dynamics (MD) simulations and atomic force microscopy (AFM) results obtained from widely used imidazolium based ionic liquids have shown that the imidazolium ring interacts more strongly than the side-chain with the solid surface of silica[4−7] and mica.[7−910] MD simulations predict the diffusivity of imidazolium ILs is reduced as the filling fraction of the IL in the pores decreases.[11] Differential scanning calorimetry (DSC) results show the depression or disappearance of thermal phase transitions with ILs confined in mesoporous silica.[4,5,12−16] An increased T_m for an imidazolium IL confined in multiwalled carbon nanotubes has been reported.[17] Nuclear magnetic resonance (NMR) spectroscopy, including pulsed-field gradient (PFG) NMR, has been widely used to gain a molecular level understanding of ILs in bulk[18−20] and in porous media.[1,12−14,21] The confinement effect on reorientational and translational motions of liquid in porous material has been studied by NMR relaxation measurements.[22−25]

Received: May 21, 2013
Revised: July 1, 2013
Published: July 19, 2013

In this study, the rotational and translational (self-diffusion) motion of the cation of the ionic liquid 1-butyl-3-methlyimidazolium bistrifluoromethylsulfonimide ([C_4mim][Tf_2N]) (**1**) was measured for the bulk liquid and for the liquid confined within mesoporous silica, KIT-6 (pore diameter = 9.5 nm[26]), as a function of filling factor f = ~0.11−1, where f = 1 represents complete filling of the pore volume. The rotational correlation times, calculated using Bloembergen−Purcell−Pound (BPP) theory[27] from ^{1}H spin−lattice relaxation times, T_1, and the self-diffusion coefficient of the cation $[C_4mim]^+$, measured by ^{1}H pulsed-field gradient NMR (PFG-NMR), were used to infer the distribution of **1** in the partially filled pores of this silica.

EXPERIMENTAL SECTION

Materials. The mesoporous silica, KIT-6, used in this study was synthesized as previously reported.[26] It has a bicontinuous gyroid pore structure with a 9.5 nm pore diameter, 783 $m^2 \cdot g^{-1}$ surface area and 1.11 $cm^3 \cdot g^{-1}$ pore volume. The IL [C_4mim][Tf_2N], **1**, was synthesized from methylimidazole in two steps, according to literature procedures.[28] The f = 1 sample is designated **1**-Si_V. Partially filled samples with f = 0.44, 0.22, and 0.11, are designated **1**-Si_M, **1**-$Si_{M/2}$, **1**-$Si_{M/4}$, respectively, as the loading level roughly corresponds to the stoichiometric concentration required to form a monolayer or fractional monolayer in the mesoporous silica, as indicated. **1**-Si_V was prepared by adding KIT-6, 144 mg, to an ethanol solution containing 227 mg of **1**. After stirring the heterogeneous solution for 1 h, ethanol was removed at 80 °C using vacuum (20 mmHg) for 24 h. The amount of [C_4mim][Tf_2N] required to prepare **1**-Si_V was calculated using the silica pore volume and the density of **1**, 1.43 $g \cdot cm^{-3}$. To estimate the loading amount of **1** needed to prepare the series of partially filled samples we used the surface area of KIT-6 and molecular diameter of **1**. We chose to use a molecular diameter of 1 nm for **1**, 25% larger than the 0.79 nm value measured by AFM,[9] to be certain to err on the side of lower coverage as a hedge against structural features that make this calculation imprecise. For **1**-Si_M, **1**-$Si_{M/2}$, and **1**-$Si_{M/4}$, 129, 130, and 124 mg of KIT-6 and 89, 45, 22 mg of **1** were used, respectively. The designation **1**-Si is used when referring generically to **1**-impregnated silicas.

An estimate of the mole fractions of **1** in contact with the surface vs the fraction removed from the pore surface for the **1**-Si_V sample was made geometrically. The cross-sectional area of the pore (9.5 nm) was divided into concentric annular rings 1 nm in width, the approximate molecular diameter of **1**. The annular rings hold πd molecules where d is the average diameter of the ring: d = 2, 4, 6, and 8 nm. This simple model predicts that the mole fraction in contact with the surface is 0.38. This estimate is used in the results and discussion section.

NMR Measurements. All NMR measurements were performed on a 9.4 T Bruker Avance 400 NMR spectrometer at Larmor frequencies, ν_0, of 400.1 and 100.6 MHz for ^{1}H and ^{13}C NMR, respectively. Samples (free-flowing powders) were packed into 5 mm NMR tubes and examined with conventional solution-state NMR methods, and were run in an unlocked mode. T_1 and spin−spin relaxation, T_2, were measured using inversion recovery (180°−τ−90°−acquire) and Carr−Purcell−Meiboom−Gill pulse sequences, respectively.[29,30]

Rotational correlation times, τ_c, were calculated from measured T_1 values using the Bloembergen−Purcell−Pound equation[27]

$$\frac{1}{T_1} = \frac{6}{5}\left(\frac{\mu_0}{4\pi}\right)^2 \frac{\gamma^4 \hbar^2}{b^2} I(I+1)\left[\frac{\tau_c}{1+\omega_0^2\tau_c^2} + \frac{4\tau_c}{1+4\omega_0^2\tau_c^2}\right] \quad (1)$$

where μ_0 is the vacuum permeability, γ is the gyromagnetic ratio of the proton ($2\pi \times 42.576$ rad·MHz·T^{-1}), $\hbar$ is reduced Planck's constant, b (=Σr) is the distance between protons and the sum runs over all protons that are dipolar coupled to the proton evaluated, I is nuclear spin number of the proton (=1/2), $\omega_0 = 2\pi\nu_0$, and τ_c is the rotational correlation time. T_1s are determined as a function of temperature. The condition $\omega_0\tau_c \approx 0.616$ applies at the T_1 minimum ($T_{1\,min}$) and is used to evaluate the rotational correlation time appropriate for the temperature at the minimum: $\tau_c = 2.45 \times 10^{-10}$ s.[27] At the minimum, b is evaluated as the only unknown in eq 1. The distance term is assumed constant as a function of temperature and used to calculate τ_c at all temperatures. The $T_{1\,min}$ of H6 in **1** (Scheme 1) occurs at 285 K. We associate this minimum with overall molecular reorientation of the ring and use this temperature for the unobserved minimum for the ring protons.

Scheme 1. [C_4mim][Tf_2N], 1; the Numerals Label the Carbon and Implicit Proton Resonances

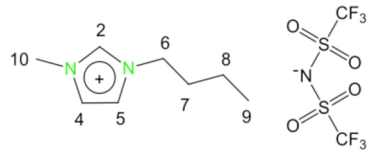

Diffusion. D was measured with the stimulated echo bipolar pulse-gradient pulse (stebpgp) sequence. The gradient strength was varied in 16 equal steps from 2 to 95% of the maximum gradient strength of the probe, 54.4 ± 0.3 $G \cdot cm^{-1}$, determined by a ^{1}H magnetic resonance imaging method.[30,31] The stimulated echo height decays were fit to the equation $S(g) = S(0)\exp[-D(\gamma\delta g)^2(\Delta - \delta/3)]$. Here, $S(g)$ and $S(0)$ are the echo heights at gradient strength g and 0, respectively. D is diffusion coefficient, γ is the gyromagnetic ratio of ^{1}H, δ is gradient-pulse length, and Δ is the duration between the two gradient pulses, i.e, the diffusion time in the experiment.[32] The Δ dependence of the diffusion coefficient as a function of temperature was measured with δ fixed at 16 ms. This is the longest gradient pulse length used in the experimental protocol to measure D, chosen to minimize errors from sample convection due to temperature gradients induced by the gradient pulse. The effects of temperature gradient were evaluated using specially designed sample tubes[33] and/or pulse sequences.[34] Errors generated by insufficient echo decay using short diffusion times are negligible in this experiment (see Figure 1S in Supporting Information).

It is well-known that in heterogeneous media the apparent diffusion coefficient (D_{app}) can be lower than the actual value from coupling between applied and internal gradients.[35,36] It is the cross-term between these gradients in the attenuated spin echo signal that introduce error into the determination of D. Bipolar magnetic field gradients are used to suppress the cross-term, but their effectiveness assumes a constant internal gradient.[37] In fast diffusion and/or at long Δ, the displacement is long enough that diffusing molecules experience a changing gradient. The elimination of the cross-term in this situation has been effected by replacing the conventional bipolar gradient pulses with gradient pulses with specific pulsed field gradient

dx.doi.org/10.1021/jp404990q | J. Phys. Chem. C 2013, 117, 15754−15762

amplitude ratios that depend only on the pulse sequence timing and not on sample properties, so-called magic pulsed field gradient (MPFG) pulse sequences.[38] The magnetic flux density gradient, ΔB, was estimated at 0.3 gauss in the pores of KIT-6 due to magnetic susceptibility inhomogeneity between the center of the pore and the silica surface (see next section). In view of this gradient, the diffusion coefficients from the MPFG experiment and the stimulated echo bipolar pulse-gradient pulse (stebpgp) sequence have been compared for the **1**-Si$_V$ sample. Within the parameter space of this study, no internal gradient effect on the determination of D_{app} was observed.

RESULTS AND DISCUSSION

The ^{1}H and ^{13}C NMR spectra obtained from neat **1** and silica-confined **1** (**1**-Si$_X$, X = V, M, M/2, and M/4) are presented in Figure 1. The eight peaks in the ^{1}H spectrum of **1** are assigned

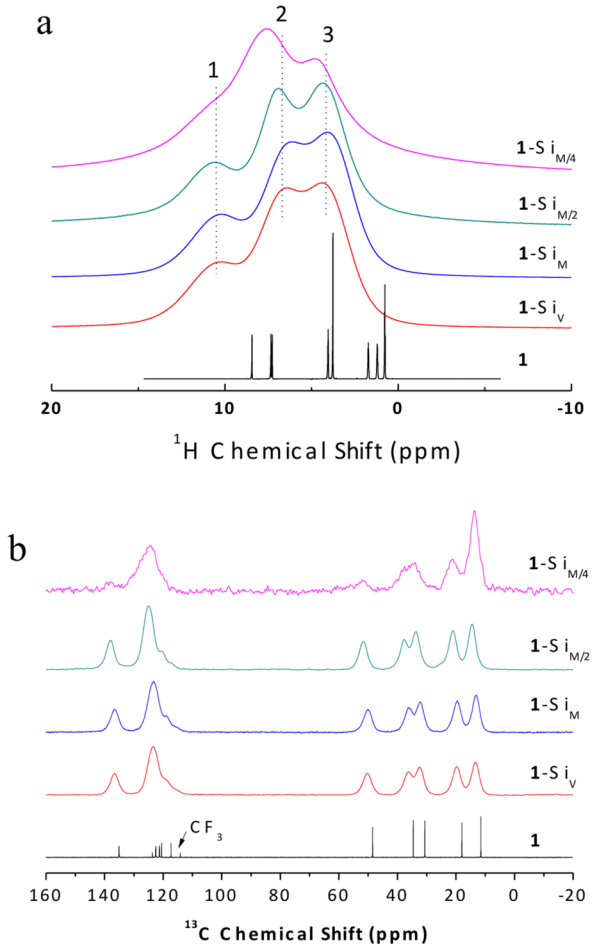

Figure 1. ^{1}H (a) and ^{4613}C (b) NMR spectra of neat [C_4mim][Tf_2N], **1**, and silica confined **1** as a function of filling factor: volume-filled (**1**-Si$_V$), monolayer (**1**-Si$_M$), half-monolayer (**1**-Si$_{M/2}$), and quarter-monolayer (**1**-Si$_{M/4}$) samples. The ^{13}C NMR spectrum of **1** shows the ^{19}F-coupled quartet from the CF_3 peak of the [Tf_2N] anion.

to H2, H5, H4, H6, H10, H7, H8, and H9 from left to right (see the numbering on the chemical structure in Scheme 1). The H5 and H4 resonances are too close to resolve at the scale used in Figure 1a. The ^{1}H spectra of the silica-confined samples consist of three broad peaks, **1**-Si$_X$-1, -2, and -3 (X = V, M, M/2, and M/4) from left to right, assigned to the imidazolium ring (H2, H4, and H5), N−CH_3/N−CH_2 (H10 and H6), and side-chain positions (H7, H8, and H9), respectively. The line width of these ^{1}H spectra is similar to those previously reported for [C_4mim][Tf_2N] in silica pores.[1,13,14,21] The spectral resolution is sufficient to allow us to monitor the response of the ring, side-chain, and N−CH_3/N−CH_2 groups in the confined samples. The spectra show the resonances of **1** in the silica pores broaden and shift to low field with respect to the neat spectrum of **1**. These effects primarily arise from magnetic susceptibility (χ) differences between **1** and the silica surface, and to a lesser extent, heterogeneous chemical shift distributions in the silica pores. Magnetic susceptibility is strongly correlated with the size and shape of the silica pore.[39] The relationship between line-width and relaxation time is shown in eq 2[29]

$$\frac{1}{T_2^*} = \frac{1}{T_2} + \frac{\gamma \Delta B}{2} \text{ and } \Delta\nu_{1/2} = \frac{1}{\pi T_2^*} \quad (2)$$

where γ is the gyromagnetic ratio of ^{1}H ($2\pi \times 42.576$ rad·MHz·T^{-1}) and of ^{13}C ($2\pi \times 10.705$ rad·MHz·T^{-1}), T_2* is transverse phase memory time including field inhomogeneity, and T_2 is the transverse nuclear relaxation time. The magnetic field inhomogeneity (ΔB) of the silica pore was estimated to be ≤0.3 gauss using ^{1}H T_2 (7 = ms) and line width ($\Delta\nu_{1/2}$ = 1.38 kHz) of the imidazolium ring resonance (**1**-Si$_M$-1) in the ^{1}H spectrum of **1**-Si$_M$. In similar fashion, ΔB was estimated to be 0.31 ± 0.02 gauss from the ^{13}C spectrum of **1**-Si$_M$ and its T_2 (See Figure 1b and Table 1S, Supporting Information).

The line width and peak position obtained from deconvolution of the three partially resolved peaks in Figure 1a are summarized in Figures S2 and S3, Supporting Information. To a first approximation, peak positions in **1**-Si$_X$ (X = V, M, and M/2) are constant. In contrast, the spectrum of **1**-Si$_{M/4}$ shows peaks 1 and 2 are displaced ca. 0.5 ppm downfield with respect to the other **1**-Si samples. Concurrently, the line widths of the resonances in **1**-Si$_{M/4}$ increase abruptly. These responses are both expected if **1** more closely approaches the silica wall surface. These qualitative observations are used in conjunction with T_2 calculations below to suggest that **1** in **1**-Si$_{M/4}$ is distributed as a thin film on the silica.

^{1}H T_2. The temperature dependence of the ^{1}H T_2 for **1**, **1**-Si$_V$, and **1**-Si$_M$, presented in Figure 2, shows typical liquid-like behavior for all samples.[27,29] The plateau on the low temperature side of the T_2 minimum is evidence for a transition to a rigid lattice (solid state). This transition occurs near 210 K in **1**-Si$_V$, **1**-Si$_M$, and **1**, not coincident with known phase transitions and ca. 20−30 degrees higher temperature than the glass transition temperature (T_g =184 K) measured in bulk **1**.[12] Precise correspondence between T_g and the T_2 minimum is not necessarily expected since DSC and NMR measure very different responses of the sample, though both are expected to be sensitive to the solid/liquid phase transition. The T_2 results show that silica confined **1** preserves liquid-like properties in the silica pore.[11,13,14] The relaxation time of **1** in contact with the surface ($T_{2,s}$) can be estimated using the two-state fast exchange model, eq 3

$$\frac{1}{T_2} = \frac{\alpha}{T_{2,b}} + \frac{(1-\alpha)}{T_{2,s}} \quad (3)$$

where T_2 is the measured T_2 of **1**-Si$_V$, $T_{2,b} = T_2$ of **1**, and $(1-\alpha)$ is the mole fraction of molecules in contact with the silica surface (0.38 in **1**-Si$_V$, see the experimental section). Using T_2 of **1**-Si$_V$ at 300 K (13 ms) and $T_{2,b} \approx 500$ ms, $T_{2,s}$ is estimated at

dx.doi.org/10.1021/jp404990q | J. Phys. Chem. C 2013, 117, 15754−15762

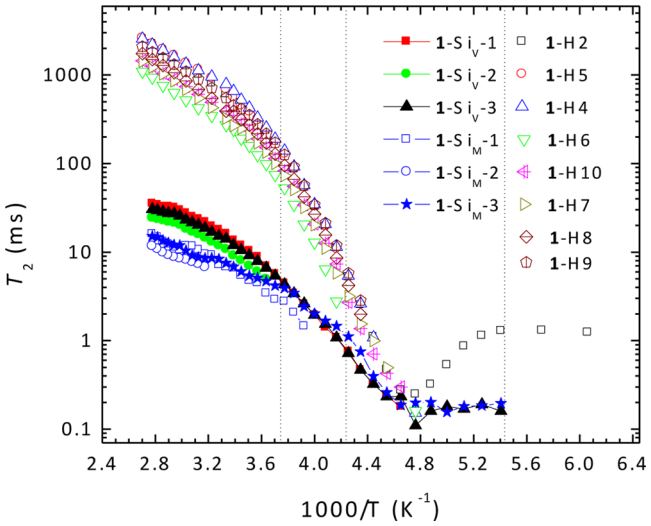

Figure 2. Temperature dependence of T_2 of ^{1}H NMR of neat **1** and silica confined [C_4mim][Tf_2N]. The vertical dotted lines indicate melting (T_m), crystallization (T_{XL}), and glass transition (T_g) temperatures, from left to right.

5 ms. The value is in fair agreement with the T_2 measured from the **1**-$Si_{M/4}$ sample (1.3 ms). This result and the obvious change in line width of the **1**-$Si_{M/4}$ cation resonances (in both^1 H and ^{13}C spectra) point to a profound change in the dynamics and ordering of **1** on the surface.

^{1}H T_1. The temperature dependence of the spin−lattice relaxation time, T_1, of bulk and silica-confined [C_4mim][Tf_2N] are presented in Figure 3a,b, respectively. The neat liquid shows the response expected for a liquid in the high temperature regime, $T_1 = T_2$ (compare Figures 2 and 3a). The relaxation response is different for **1**-Si where T_2 is 1−2 orders of magnitude shorter than the T_1 in the high temperature region. This relaxation pattern on silica is consistent with a two-dimensional (2D) relaxation theory that incorporates strong interactions between confined liquids and the solid surface and includes fast exchange between the surface and bulk phases.[22−25] The theory predicts high-frequency relaxation (T_1) is less sensitive to the effects of geometrical confinement than low-frequency relaxation processes, spin−spin (T_2) and spin−lattice relaxation in the rotating frame ($T_{1\rho}$). T_2 of the **1**-Si_V and **1**-Si_M samples differ in the high temperature region, whereas T_1 exhibits little discrimination between these samples (compare Figures 2 and 3b). Compound **1**-Si shows typical 2D liquid relaxation behavior: $T_2 \ll T_1$ and $T_{1\rho} \ll T_1$ in the extreme narrowing limit ($\omega_0\tau_C \ll 1$) and a linear dependence of T_1^{-1} and $T_{1\rho}^{-1}$ on log ω,[22,24] in contrast to bulk [C4mim][Tf2N], for which $T_2 = T_{1\rho} = T_1$. The frequency-dependent $T_{1\rho}^{-1}$ and T_1^{-1} correlation shown in Figure 4 is excellent evidence that a 2D model for relaxation in **1**-Si is apt.[22]

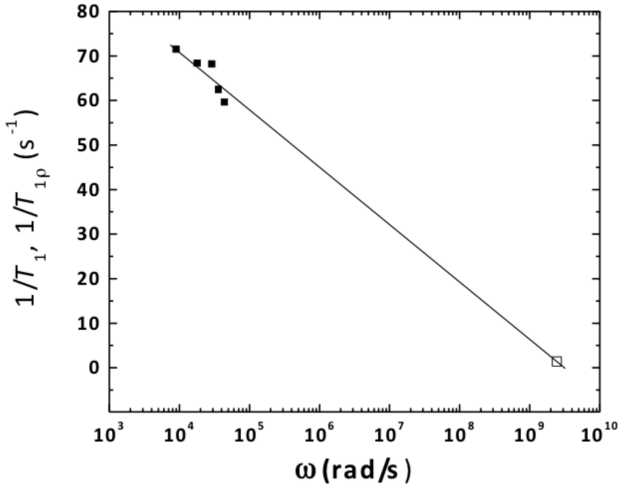

Figure 4. ^{1}H T_1^{-1} (□) and $T_{1\rho}^{-1}$ (■) as a function of log ω for **1**-Si_M at 295 K. The line is a guide for the eye.

The T_1 relaxation curves for **1** in the mesoporous silica show single exponential decay, evidence of fast exchange between molecules on the surface and in the bulk.[25] This dynamic heterogeneity between populations averages T_1 and obscures the relaxation drivers. The T_1 of **1**-Si may be strongly influenced by surface relaxation effects. The ^{1}H T_1 of the exchange-averaged hydroxyl and water resonances of the solid mesoporous KIT-6 are 0.7 and 0.8 s at 294 K for samples

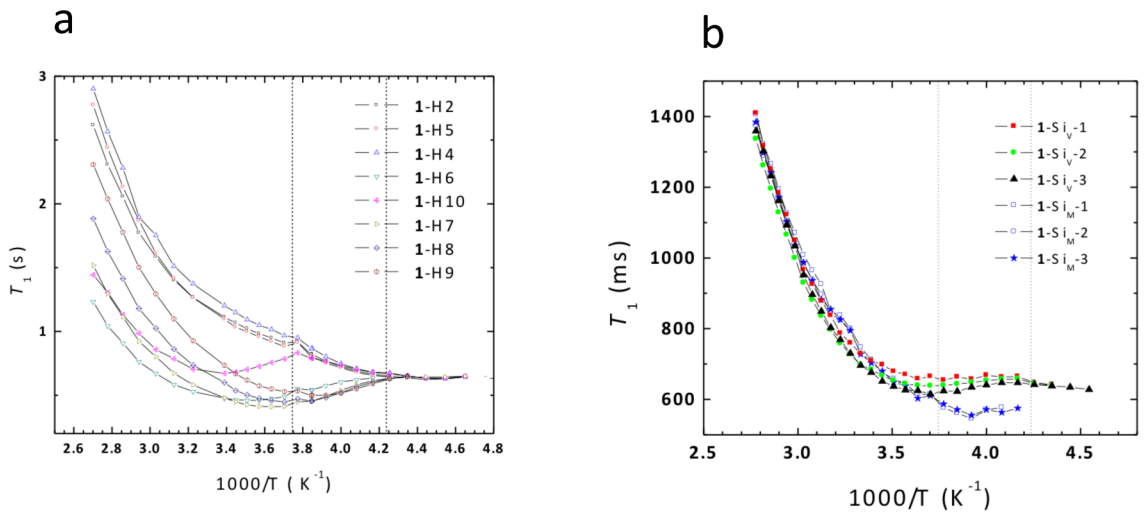

Figure 3. Temperature dependence of T_1 of ^{1}H NMR of **1** (a) and **1**-Si_V and **1**-Si_M (b). The vertical dotted lines indicate the melting (T_m) and crystallization (T_{XL}) temperatures, from left to right.

dx.doi.org/10.1021/jp404990q | J. Phys. Chem. C 2013, 117, 15754−15762

exposed to ambient humidity and vacuum drying, respectively. These T_1 values are similar to the T_1 of the cation resonances of **1**-Si_V (0.7 s) and **1**-Si_M (0.7 s) at the same temperature. This accidental degeneracy of T_1 for these systems does not allow us to conclude that the surface strongly directs relaxation through translational motion on the surface. Nonetheless, relaxation by surface dipoles remains a likely mechanism depending on the correlation time for reorientation on the surface.[40]

^{1}H T_1 in Neat 1. The temperature dependence of the site specific ^{1}H T_1s in **1** are shown in Figure 3a. The N−CH_3 and side chain resonances show well-defined T_1 minima. All curves show a discontinuity in the data very close to the known melting temperature of the IL, 267 K. This causes a local discontinuity in the T_1 curves that directly impacts the data analysis. The same effect is seen on the relaxation curve for the N−CH_3 resonance, H10, calling into doubt the data point(s) near the melting temperature. The discontinuity should have little effect on the T_1 response far from the transition. Hence, the minimum seen for the N−CH_3 resonance occurring at 295 K, 30 K higher temperature than T_m, appears unrelated to phase change behavior associated with T_m, and must represent a true localized T_1 minimum for this resonance. The minimum is associated with the unique motion of the methyl group, rotation about its C−N axis. The T_1 for this motion reaches its minimum value (for which $\tau_0 = 2.45 \times 10^{-10}$ s) first, implying that this motion is the slowest, i.e., has the highest activation energy, in comparison to remaining molecular motions (overall molecular reorientation, segmental motion of the side chain, C-methyl group rotation, etc.). At the temperature of the discontinuity, the N−CH_3 relaxation curve adopts the trajectory of the ring proton T_1s and continues to decrease toward a second minimum as the temperature decreases. This second minimum is not well-defined since the T_1 minimum is not reached prior to the crystallization temperature of **1** where all the resonances coalesce. It is clear, nonetheless, that the ring proton resonances participate in a local motion with a low activation energy. It is not likely to be overall molecular rotation since this process requires major nearest neighbor molecular reorientation. We suggest the low energy motion is a libration of the imidazolium ring.

The T_1-derived τ_c of **1** are presented in Figure 5. It is clear from this plot that τ_c is linear in the high temperature region, above 310 K. Segmental motion is clearly evident in the ordering of the side chain τ_c: H6 > H7 > H8 > H9. The τ_c for H6 and the ring sites H2, H4, and H5 coincide. The N−CH_3 group displays the longest correlation time in the molecule. Similar behavior was observed in other ionic liquids.[19] Recent studies of reorientational dynamics in [C_4mim][Br] and [C_4C_1mim][Br][41] and observation of slow N−CH_3 rotation in [C_4mpip][Tf_2N][37] and [C_4mpyr][Tf_2N][42] suggests the N−CH_3 rotation is a function of cation structure. Methyl rotors are symmetric tops whose internal rotation does not require nearest-neighbor reorganization in order for the motion to proceed. This feature and their low inertial mass usually translate into fast rotation rates for C−CH_3 groups, although unusual structures incorporating steric crowding can alter their correlation times by orders of magnitude. It is this relative comparison through which the N−CH_3 rotation rates in ILs are deemed to be slow. Hence, the T_1 minimum for the N−CH_3 resonance is observed at high temperature while the corresponding minimum for the C−CH_3 group, H9, is not observed above the crystallization temperature (Figure 3a). Figure 3a and Figure 5 demonstrate that the protons of the ring

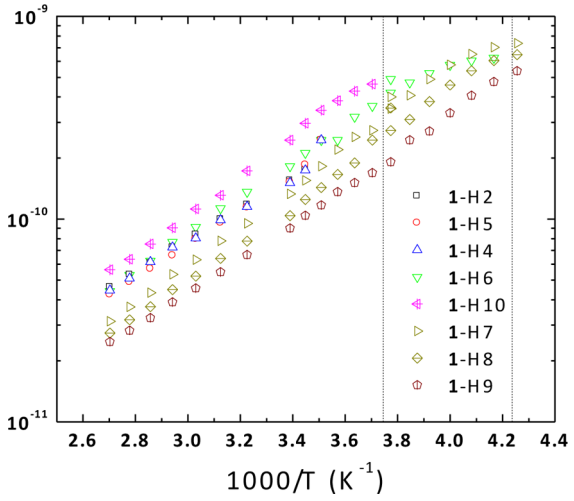

Figure 5. Temperature dependence of the reorientational correlation time of C_4mim^+ in [C_4mim][Tf_2N] calculated from the ^{1}H NMR T_1. The vertical dotted lines indicate the melting (T_m) and crystallization (T_{XL}) temperatures, from left to right.

and the N−CH_3 group show a nonlinear response over a large temperature range extending to the phase discontinuity near 260 K, indicating these protons are responding to multiple dipolar fluctuations.

Diffusion. The diffusion time (Δ) dependence of the self-diffusion coefficient obtained from **1**-Si_V and **1**-Si_M over the temperature range of 360 to 260 K is presented in Figures 6

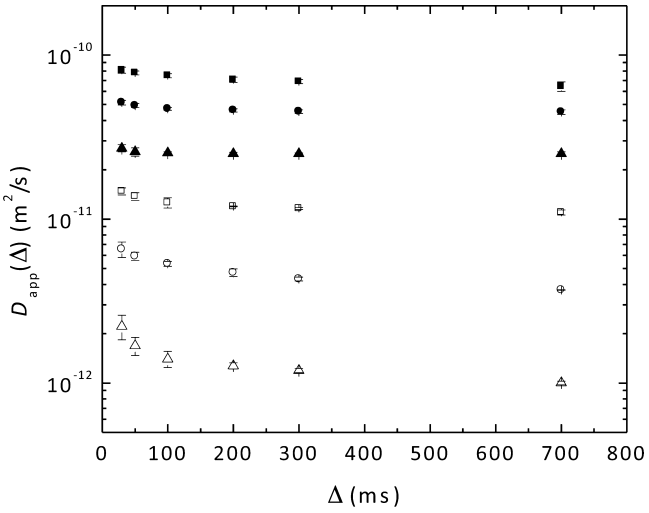

Figure 6. Δ dependence of apparent diffusion coefficient, $D_{app}(\Delta)$ of **1**-Si_V as a function of temperature: 360, 340, 320, 300, 280, and 260 K, from top to bottom. The three peaks of **1**-Si_V have the same diffusion coefficient at all measured Δ and temperatures within experimental error. The error bar shows the standard deviation of the diffusion coefficient between the three peaks.

and 7, respectively. D measured in the silica pores is dependent on experimental parameters and the specific structure of the mesoporous silica, in contrast to D measured in bulk solution, and is denoted as an apparent diffusion coefficient, D_{app}. The measured diffusion coefficient is a strong function of the diffusion time at short Δ. Extrapolated to Δ = 0, $D_{app,0}$, approaches D_0, the bulk diffusion coefficient, since for short diffusion time the mean displacement of the diffusing particle is

dx.doi.org/10.1021/jp404990q | J. Phys. Chem. C 2013, 117, 15754−15762

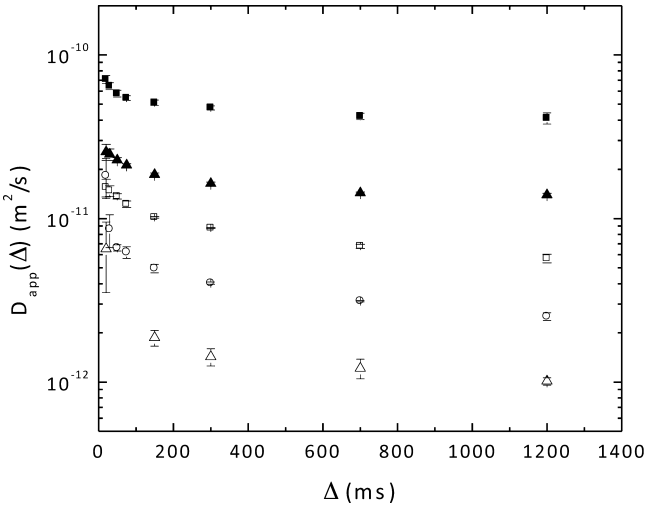

Figure 7. Δ dependence of apparent diffusion coefficient, $D_{app}(\Delta)$ of **1**-Si_M as a function of temperature: 360, 320, 300, 280, and 260 K, from top to bottom. The three peaks of **1**-Si_M have the same diffusion coefficient at all measured Δ and temperatures within experimental error. The error bar shows the standard deviation of the diffusion coefficient between the three peaks.

short compared to the dimensions of the diffusion space.[43,44] At long Δ, the diffusion coefficient asymptotically approaches a lower, steady-state value, $D_{app,\infty}$, dependent upon the geometry and pore size of the silica, and defined in relation to the bulk diffusion coefficient as the tortuosity, $\mathcal{T}$, where $\mathcal{T} \equiv D_0/D_{app,\infty}$. In this work, $D_{app,\infty}$ is approximated by the value of $D_{app,\Delta}$ at the longest measured Δ.

The temperature dependence of D_0 for **1** and $D_{app,\infty}$ for **1**-SI_V, **1**-SI_M, and **1**-$Si_{M/2}$ is presented in Figure 8. Diffusion data

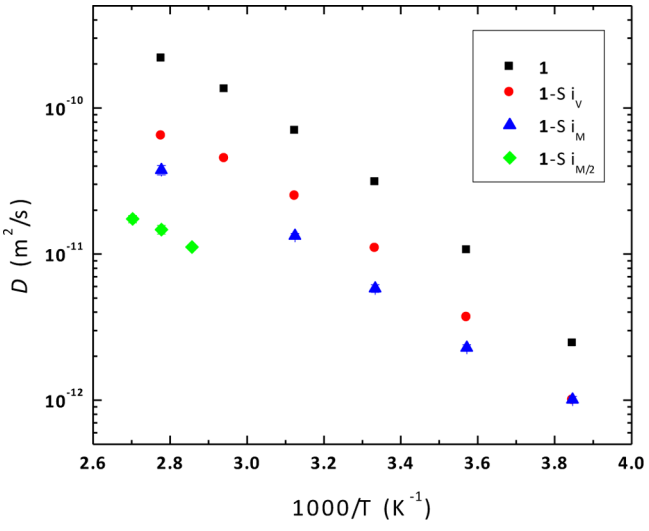

Figure 8. Temperature dependence of D_0 and steady-state $D_{app}(\Delta = \infty)$ of **1**-Si_V, **1**-Si_M, and **1**-$Si_{M/2}$.

for **1**-$Si_{M/4}$ could not be measured since the shortened relaxation times of this sample defeated the characterization of the echo decay from the diffusion process. $D_{app,\infty}$ for the **1**–Si samples shows a temperature dependence similar to bulk **1** and decreases as the filling factor of the silica decreases. Figure 9 shows the linear relationship between D and T/η predicted by the Stokes–Einstein theory of diffusion, $D = k_BT/6\pi\eta r_s$,

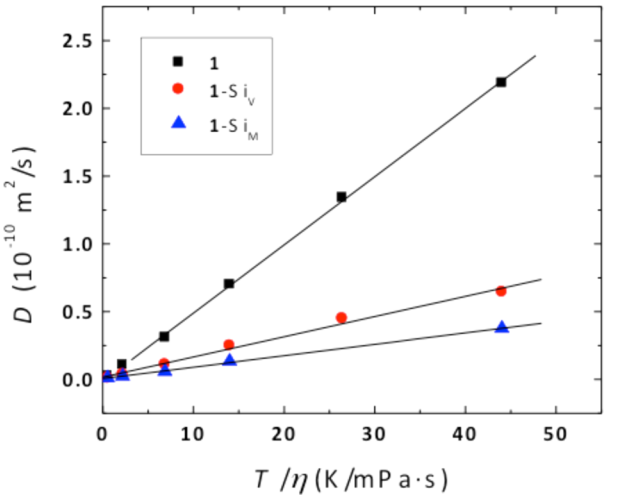

Figure 9. Diffusion coefficients, D_0, for neat **1**, and $D_{app,\infty}$, for **1**-Si samples, plotted vs T/η demonstrate conformity to the Stokes–Einstein equation.

where k_B is the Boltzmann constant, T is the absolute temperature, η is the viscosity, and r_s is hydrodynamic radius of the molecule. Figures 8 and 9 demonstrate that **1** diffuses slowly on the silica surface, in agreement with previous MD simulations for the diffusion coefficient as a function of the IL loading in silica pores.[11,45]

Filling Mode. An estimate of the mole fraction of bulk and surface molecules in the filled pore was made from a geometric model assuming the nominal pore size of KIT-6 and a spherical 1.0 nm molecular diameter for **1**. The mole fraction of the ionic liquid in contact with the silica surface is 0.38 (see the experimental section). This estimate corresponds to the distribution anticipated for the homogeneously filled silica, **1**-Si_V.

The NMR diffusion experiment measures the average D of **1** in the pore. The variation of D within concentric annular layers in the pore has been evaluated in a previous MD study of this **1**-KIT-6 system.[45] Diffusion coefficients for layers of **1** in the pore in this study correspond to the geometric model described in the experimental section. For the present purpose, we note that D for the surface layer of **1** from the MD simulation is 4×10^{-12} m^2/s; the average of the bulk layers cluster near 1×10^{-10} m^2/s.[45] Using these two MD values for D and the mole fraction of **1** in contact with the surface from the geometric model, we can compare the predicted average D from the MD simulation with the experimental D from NMR (Table 1). For **1**-Si_V (f = 1), the measured D and the MD-predicted D are in excellent agreement. This concurrence validates the MD-simulated D for surface-bound **1**, a measurement that could not be obtained experimentally, and suggests that the surface and in-pore bulk diffusion coefficients obtained from the MD simulation can be used to evaluate the unknown distribution of **1** in the $f < 1.0$ samples. The results are given in Table 1 for the **1**-Si_M and **1**-$Si_{M/2}$ samples, where the mole fractions are estimated as $x(D_{\text{MD-IN PORE BULK}}) + (1 - x)(D_{\text{MD-SURFACE}}) = D_{\text{NMR}}$.

If the sample filling were represented by stretches of filled mesopores with otherwise empty pores, then for any filling factor less than one we would anticipate the measured diffusion would equal that for **1**-Si_V since D is independent of the length of the pore, l, at macroscopic lengths, $l \gg (D\Delta)^{0.5}$. The measured D decreases with filling factor; it must be an averaged

dx.doi.org/10.1021/jp404990q | J. Phys. Chem. C 2013, 117, 15754–15762

Table 1. Mole Fractions of Surface (Layer 1) and Bulk (Layers 2−5) Populations from Measured *D* (NMR) and Calculated *D* (MD)[a] (360 K)

sample	filling fraction *f*	predicted *D* MD/model	measured *D* NMR	mole fraction layers 2−5[a]	mole fraction layer 1[a]
1	bulk		2.2×10^{-10}		
1-Si_V	1	6.4×10^{-11}	6.4×10^{-11}	0.62[b]	0.38[b]
1-Si_M	0.44		3.8×10^{-11}	0.36[c]	0.64[c]
1-$Si_{M/2}$	0.22		1.5×10^{-11}	0.12[c]	0.88[c]

[a]Calculations use $D = 4 \times 10^{-12}$ m^2/s and 1×10^{-10} m^2/s for the surface (layer 1) and in-pore bulk (layers 2−5) values, respectively, determined by MD simulation.[45] [b]For this homogeneous sample, the mole fraction is derived from the geometric model described in the experimental section. [c]These values are determined using the layer values and the experimental *D* from NMR.

value reflecting different environments for **1** in the pores. Consider the model where *D* is a weighted average of the *D* for **1**-Si_V and the *D* for the first layer coverage, i.e., a model in which the pores are either filled (**1**-Si_V, $D = 6.4 \times 10^{-11}$ m^2/s) or covered with a monolayer of **1** ($D = 4 \times 10^{-12}$ m^2/s). The mole fractions calculated for these two distribution modes are given in Table 2.

Table 2. Mole Fractions of Filled and Surface-Coated Distributions from Measured *D* (NMR) and Calculated *D* (MD) (360 K) for a Heterogeneous Distribution of 1 in KIT-6

			mole fractions	
sample	filling fraction *f*	measured *D* NMR	filled pore	monolayer
1-Si_V	1.0	6.4×10^{-11}	1.0	0
1-Si_M	0.44	3.8×10^{-11}	0.6[a]	0.4[a]
1-$Si_{M/2}$	0.22	1.5×10^{-11}	0.2[a]	0.8[a]
1-$Si_{M/4}$	0.11			1 (extrapolated)

[a]Calculations use the experimental $D = 6.4 \times 10^{-11}$ m^2/s for the filled pore (**1**−Si_V) and 4×10^{-12} m^2/s for the surface (layer 1) determined by MD simulation.[45]

The reversal in mole fractions for the two populations with decreasing filling factor is evident in Table 2. The mole fraction coverage in the $f = 0.22$ sample shows that there is a high propensity for **1** to form a monolayer film in the silica at low loading levels. Nonetheless, at this filling factor, two populations with different *D* exist and undergo dynamic exchange, evidenced by the similarity of the ^1H and ^{13}C spectra for the $f = 2$−1.0 samples (see Figure 1). At the lowest filling factor ($f = 0.11$, **1**−$Si_{M/4}$), diffusion data from NMR is unattainable due to short T_2. However, the qualitative change indicated by the dramatic increase in line widths (shortened T_2) in the spectra of **1**−$Si_{M/4}$, and the trend toward monolayer coverage in Table 2 suggests that **1** is not involved in dynamic exchange but is disbursed as a film on the silica surface. The film is considered a monolayer since this arrangement effectively prohibits facile exchange with nonsurface species. Monolayer coverage is consistent with the MD simulation that uses ca. 1 molecular diameter (1 nm) for the layer thickness. This analysis is the basis for the extrapolated mole fraction value for the $f = 0.11$ sample in Table 2.

Independent of the details of filling mode, the diffusion data establish that at low coverage the silica will initially have a monolayer coverage of **1**. The foregoing analysis considers the system with either filled pores or pores with a monolayer coverage, corresponding to the *D* extrema from the MD simulation (model 1). In terms of filling mode, this would correspond to additional **1** completely filling pores as added. This model provides a convenient way to parse the diffusion data but does not necessarily correspond to physical reality. The pores could also fill by increasing the layer depth of the initial surface layer, i.e., filling the pores from the wall inward (model 2). The NMR analysis from $D_{app,\infty}$ is compatible with either filling model within the approximation of this article, i.e., that layers 2−5 have the same *D*.

The models differ significantly in the cross-sectional area at the boundary between the two populations. Model 1 will possess a limited cross-sectional boundary that could impede efficient molecular exchange between populations. Model 2 maximizes the boundary area. Rapid exchange is possible if the two populations are in direct, intimate contact, a property of model 2. Support for model 2 is shown in Figure 10, which

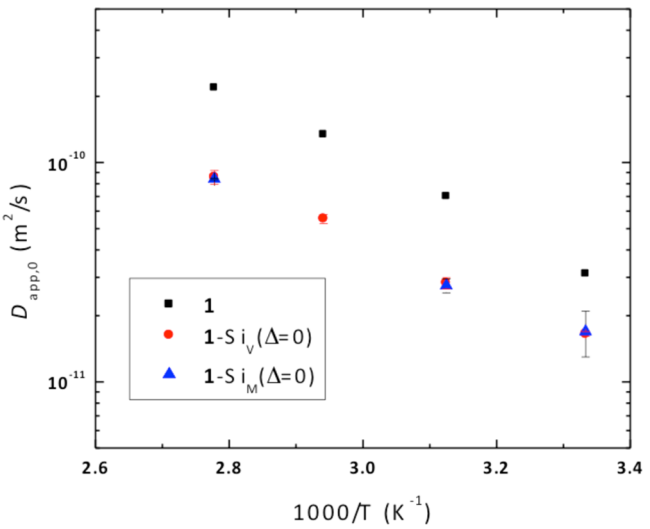

Figure 10. Temperature dependence of D_0 and $D_{app,0}$ of **1**-Si_V and **1**-Si_M, obtained by extrapolation of Δ to 0. $D_{app,0}$ is smaller than D_0 at high temperature and approaches D_0 below 300 K.

depicts the temperature dependence of $D_{app,0}$ for **1**-Si_V and **1**-Si_M. In contrast to $D_{app,\infty}$ (Figure 8) where the differences in **1**-Si_V and **1**-Si_M are substantial, $D_{app,0}$ track each other perfectly for all temperatures. This is the expected result if the pores fill from the wall inward since the short-term diffusion dynamic response of **1**-Si_V and **1**-Si_M will be nearly identical. These considerations lead to the following description of the **1**-Si system: at low filling factors **1** has a strong propensity to form a monolayer on the mesoporous silica surface. The interaction energy for **1** with the surface is greater than the self-association energy of **1**. At higher filling fractions, additional **1** accumulates on the surface layer forming the population away from the surface. The two molecular environments are in fast exchange

dx.doi.org/10.1021/jp404990q | J. Phys. Chem. C 2013, 117, 15754−15762

with respect to both translational diffusion and rotational relaxation times of the surface and bulk populations of **1**.

CONCLUSIONS

Rotational correlation times and diffusion coefficients of the cation of the bulk and silica confined ionic liquid $[C_4mim][Tf_2N]$ have been measured. The rotational and translational motions of $[C_4mim]^+$ are reduced at the silica surface. Susceptibility inhomogeneity in the silica pores, which was estimated to be 0.3 gauss from ^1H and ^{13}C spectrum and T_2, does not influence the measured diffusion coefficients. Temperature dependent T_2 show that **1** in the pores of KIT-6 remains liquid-like 50 K below the bulk melting point. In conjunction with MD simulations that provide an experimentally testable diffusion value for **1** on the surface of KIT-6, the diffusion times from PFG ^1H NMR allow an estimate of the mole fractions of fast (bulk) and slow (slow) populations of **1** in partially filled silicas. Measured D in the limit of short and long diffusion times permit a distinction to be made on filling mode: at low filling fraction, the ionic liquid **1** disperses over the silica surface to form a monolayer of **1**. As the filling fraction increases, **1** is built up on the surface layer forming an increasingly thick layer of **1**.

ASSOCIATED CONTENT

Supporting Information

Error analysis in diffusion measurements and deconvoluted ^1H spectra of **1**-Si samples. This material is available free of charge via the Internet at http://pubs.acs.org.

AUTHOR INFORMATION

Corresponding Author

*(E.W.H.) Tel: 865-576-2751. Fax: 865-576-7956. E-mail: hagamanew@ornl.gov.

Notes

The authors declare no competing financial interest.

ACKNOWLEDGMENTS

This work was supported by the Fluid Interface Reactions, Structures, and Transport (FIRST) Center, an Energy Frontier Research Center funded by the U.S. Department of Energy, Office of Science, Office of Basic Energy Sciences.

REFERENCES

(1) Le Bideau, J.; Viau, L.; Vioux, A. Ionogels, Ionic Liquid Based Hybrid Materials. *Chem. Soc. Rev.* **2011**, *40*, 907−925.

(2) Armand, M.; Endres, F.; MacFarlane, D. R.; Ohno, H.; Scrosati, B. Ionic-Liquid Materials for the Electrochemical Challenges of the Future. *Nat. Mater.* **2009**, *8*, 621−629.

(3) Weingärtner, H. Understanding Ionic Liquids at the Molecular Level: Facts, Problems, and Controversies. *Angew. Chem., Int. Ed.* **2008**, *47*, 654−670.

(4) Liu, Y.; Wu, G.; Fu, H.; Jiang, Z.; Chen, S.; Sha, M. Immobilization and Melting Point Depression of Imidazolium Ionic Liquids on the Surface of Nano-SiO_x Particles. *Dalton Trans.* **2010**, *39*, 3190−3194.

(5) Singh, M. P.; Singh, R. K.; Chandra, S. Properties of Ionic Liquid Confined in Porous Silica Matrix. *ChemPhysChem* **2010**, *11*, 2036−2043.

(6) Rollins, J. B.; Fitchett, B. D.; Conboy, J. C. Structure and Orientation of the Imidazolium Cation at the Room-Temperature Ionic Liquid/SiO_2 Interface Measured by Sum-Frequency Vibrational Spectroscopy. *J. Phys. Chem. B* **2007**, *111*, 4990−4999.

(7) Atkin, R.; Warr, G. G. Structure in Confined Room-Temperature Ionic Liquids. *J. Phys. Chem. C* **2007**, *111*, 5162−5168.

(8) Bou-Malham, I.; Bureau, L. Nanoconfined Ionic Liquids: Effect of Surface Charges on Flow and Molecular Layering. *Soft Matter* **2010**, *6*, 4062−4065.

(9) Yokota, Y.; Harada, T.; Fukui, K.-I. Direct Observation of Layered Structures at Ionic Liquid/Solid Interfaces by Using Frequency-Modulation Atomic Force Microscopy. *Chem. Commun.* **2010**, *46*, 8627−8629.

(10) Hayes, R.; El Abedin, S. Z.; Atkin, R. Pronounced Structure in Confined Aprotic Room-Temperature Ionic Liquids. *J. Phys. Chem. B* **2009**, *113*, 7049−7052.

(11) Coasne, B.; Viau, L.; Vioux, A. Loading-Controlled Stiffening in Nanoconfined Ionic Liquids. *J. Phys. Chem. Lett.* **2011**, *2*, 1150−1154.

(12) Neouze, M.-A.; Bideau, J. L.; Leroux, F.; Vioux, A. A Route to Heat Resistant Solid Membranes with Performances of Liquid Electrolytes. *Chem. Commun.* **2005**, 1082−1084.

(13) Néouze, M.-A.; Bideau, J. L.; Gaveau, P.; Bellayer, S.; Vioux, A. Ionogels, New Materials Arising from the Confinement of Ionic Liquids within Silica-Derived Networks. *Chem. Mater.* **2006**, *18*, 3931−3936.

(14) Gobel, R.; Hesemann, P.; Weber, J.; Moller, E.; Friedrich, A.; Beuermann, S.; Taubert, A. Surprisingly High, Bulk Liquid-Like Mobility of Silica-Confined Ionic Liquids. *Phys. Chem. Chem. Phys.* **2009**, *11*, 3653−3662.

(15) Zhang, J.; Zhang, Q.; Li, X.; Liu, S.; Ma, Y.; Shi, F.; Deng, Y. Nanocomposites of Ionic Liquids Confined in Mesoporous Silica Gels: Preparation, Characterization and Performance. *Phys. Chem. Chem. Phys.* **2010**, *12*, 1971−1981.

(16) Waechtler, M.; Sellin, M.; Stark, A.; Akcakayiran, D.; Findenegg, G.; Gruenberg, A.; Breitzke, H.; Buntkowsky, G. ^2H and ^{19}F Solid-State NMR Studies of the Ionic Liquid $[C_2Py][BTA]$-D_{10} Confined in Mesoporous Silica Materials. *Phys. Chem. Chem. Phys.* **2010**, *12*, 11371−11379.

(17) Chen, S.; Wu, G.; Sha, M.; Huang, S. Transition of Ionic Liquid $[bmim][PF_6]$ from Liquid to High-Melting-Point Crystal When Confined in Multiwalled Carbon Nanotubes. *J. Am. Chem. Soc.* **2007**, *129*, 2416−2417.

(18) Hayamizu, K. Studies on the Translational and Rotational Motions of Ionic Liquids Composed of *N*-Methyl-*N*-propyl-pyrrolidinium (P_{13}) Cation and Bis(trifluoromethanesulfonyl)amide and Bis(fluorosulfonyl)amide Anions and Their Binary Systems Including Lithium Salts. *J. Chem. Phys.* **2010**, *133*, 194505.

(19) Hayamizu, K.; Tsuzuki, S.; Seki, S. Molecular Motions and Ion Diffusions of the Room-Temperature Ionic Liquid 1,2-Dimethyl-3-propylimidazolium bis(trifluoromethylsulfonyl)amide (DMPImTFSA) Studied by ^1H, ^{13}C, and ^{19}F NMR. *J. Phys. Chem. A* **2008**, *112*, 12027−12036.

(20) Imanari, M.; Uchida, K.-I.; Miyano, K.; Seki, H.; Nishikawa, K. NMR Study on Relationships between Reorientational Dynamics and Phase Behaviour of Room-Temperature Ionic Liquids: 1-Alkyl-3-Methylimidazolium Cations. *Phys. Chem. Chem. Phys.* **2010**, *12*, 2959−2967.

(21) Le Bideau, J.; Gaveau, P.; Bellayer, S.; Neouze, M. A.; Vioux, A. Effect of Confinement on Ionic Liquids Dynamics in Monolithic Silica Ionogels: ^1H NNR Study. *Phys. Chem. Chem. Phys.* **2007**, *9*, 5419−5422.

(22) Korb, J. P.; Xu, S.; Jonas, J. Confinement Effects on Dipolar Relaxation by Translational Dynamics of Liquids in Porous Silica Glasses. *J. Chem. Phys.* **1993**, *98*, 2411−2422.

(23) Korb, J. P.; Delville, A.; Xu, S.; Demeulenaere, G.; Costa, P.; Jonas, J. Relative Role of Surface Interactions and Topological Effects in Nuclear Magnetic Resonance of Confined Liquids. *J. Chem. Phys.* **1994**, *101*, 7074−7081.

(24) Liu, G.; Li, Y.; Jonas, J. Confined Geometry-Effects on Reorientational Dynamics of Molecular Liquids in Porous Silica Glasses. *J. Chem. Phys.* **1991**, *95*, 6892−6901.

(25) Mattea, C.; Kimmich, R.; Ardelean, I.; Wonorahardjo, S.; Farrher, G. Molecular Exchange Dynamics in Partially Filled

Microscale and Nanoscale Pores of Silica Glasses Studied by Field-Cycling Nuclear Magnetic Resonance Relaxometry. *J. Chem. Phys.* **2004**, *121*, 10648−10656.
(26) Morishige, K.; Tarui, N. Capillary Condensation of Nitrogen in Ordered Mesoporous Silica with Bicontinuous Gyroid Structure. *J. Phys. Chem. C* **2007**, *111*, 280−285.
(27) Abragam, A. *The Principles of Nuclear Magnetism*; Oxford University Press: New York, 1961.
(28) Burrell, A. K.; Sesto, R. E. D.; Baker, S. N.; McCleskey, T. M.; Baker, G. A. The Large Scale Synthesis of Pure Imidazolium and Pyrrolidinium Ionic Liquids. *Green Chem.* **2007**, *9*, 449−454.
(29) Farrar, T. C.; Becker, E. D. *Pulse and Fourier Transform Nmr: Introduction to Theory and Methods*; Academic Press Inc.: New York, 1971.
(30) Fukushima, E.; Roeder, S. B. W. *Experimental Pulse NMR: A Nuts and Bolts Approach*; Addision-Wesley Publishing Company: Reading, MA, 1981.
(31) Yadav, N. N.; Torres, A. M.; Price, W. S. An Improved Approach to Calibrating High Magnetic Field Gradients for Pulsed Field Gradient Experiments. *J. Magn. Reson.* **2008**, *194*, 25−28.
(32) Johnson, C. S., Jr. Diffusion Ordered Nuclear Magnetic Resonance Spectroscopy: Principles and Applications. *Prog. Nucl. Magn. Reson. Spectrosc.* **1999**, *34*, 203−256.
(33) Hayamizu, K.; Price, W. S. A New Type of Sample Tube for Reducing Convection Effects in PGSE-NMR Measurements of Self-Diffusion Coefficients of Liquid Samples. *J. Magn. Reson.* **2004**, *167*, 328−333.
(34) Jerschow, A.; Müller, N. Suppression of Convection Artifacts in Stimulated-Echo Diffusion Experiments. Double-Stimulated-Echo Experiments. *J. Magn. Reson.* **1997**, *125*, 372−375.
(35) Seland, J. G.; Sørland, G. H.; Zick, K.; Hafskjold, B. Diffusion Measurements at Long Observation Times in the Presence of Spatially Variable Internal Magnetic Field Gradients. *J. Magn. Reson.* **2000**, *146*, 14−19.
(36) Zheng, G.; Price, W. S. Suppression of Background Gradients in (B_0 Gradient-Based) NMR Diffusion Experiments. *Concepts Magn. Reson., Part A* **2007**, *30A*, 261−277.
(37) Cotts, R. M.; Hoch, M. J. R.; Sun, T.; Markert, J. T. Pulsed Field Gradient Stimulated Echo Methods for Improved NMR Diffusion Measurements in Heterogeneous Systems. *J. Magn. Reson.* **1989**, *83*, 252−266.
(38) Galvosas, P.; Stallmach, F.; Kärger, J. Background Gradient Suppression in Stimulated Echo NMR Diffusion Studies Using Magic Pulsed Field Gradient Ratios. *J. Magn. Reson.* **2004**, *166*, 164−173.
(39) Allen, S.; Mallett, M.; Smith, M. E.; Strange, J. H. Susceptibility Effects in Unsaturated Porous Silica. *Magn. Reson. Imaging* **1998**, *16*, 597−600.
(40) Zavada, Z.; Kimmich, R. The Anomalous Adsorbate Dynamics at Surfaces in Porous Media Studied by Nuclear Magnetic Resonance Methods. The Orientational Structure Factor and Levy Walks. *J. Chem. Phys.* **1998**, *109*, 6929−6939.
(41) Endo, T.; Imanari, M.; Seki, H.; Nishikawa, K. Effects of Methylation at Position 2 of Cation Ring on Rotational Dynamics of Imidazolium-Based Ionic Liquids Investigated by NMR Spectroscopy: [C_4mim]Br vs [C_4C_1mim]Br. *J. Phys. Chem. A* **2011**, *115*, 2999−3005.
(42) Guo, J.; Han, K. S.; Mahurin, S. M.; Baker, G. A.; Hillesheim, P. C.; Dai, S.; Hagaman, E. W.; Shaw, R. W. Rotational and Translational Dynamics of Rhodamine 6G in a Pyrrolidinium Ionic Liquid: A Combined Time-Resolved Fluorescence Anisotropy Decay and NMR Study. *J. Phys. Chem. B* **2012**, *116*, 7883−7890.
(43) Zielinski, L. J.; Sen, P. N. Effects of Finite-Width Pulses in the Pulsed-Field Gradient Measurement of the Diffusion Coefficient in Connected Porous Media. *J. Magn. Reson.* **2003**, *165*, 153−161.
(44) Ohkubo, T.; Kidena, K.; Ohira, A. Determination of a Micron-Scale Restricted Structure in a Perfluorinated Membrane from Time-Dependent Self-Diffusion Measurements. *Macromolecules* **2008**, *41*, 8688−8693.
(45) Song, L.; Han, K. S.; Feng, G.; Hagaman, E. W.; Vlcek, L.; Cummings, P. Dynamic and Structural Properties of Room Temperature Ionic Liquids near Silica and Carbon Surfaces. *Langmuir* **2013**, DOI: 10.1021/la401172z.